

Intramolecular vibrational energy redistribution in DCO (\tilde{X}^2A'): Classical-Quantum correspondence, dynamical assignments of highly excited states, and phase space transport

Aravindan Semparithi and Srihari Keshavamurthy

Department of Chemistry, Indian Institute of Technology, Kanpur, India 208 016

(Dated: November 1, 2018)

Intramolecular dynamics of highly excited DCO (\tilde{X}^2A') is studied from a classical-quantum correspondence perspective using the effective spectroscopic Hamiltonian proposed recently by Tröllsch and Temps (Z. Phys. Chem. **215**, 207 (2001)). This work focuses on the polyads $P = 3$ and $P = 4$ corresponding to excitation energies $E_v \approx 5100 \text{ cm}^{-1}$ and 7000 cm^{-1} respectively. The majority of states belonging to these polyads are dynamically assigned, despite extensive stochasticity in the classical phase space, using the recently proposed technique of level velocities. A wavelet based time-frequency analysis is used to reveal the nature of phase space transport and the relevant dynamical bottlenecks. The local frequency analysis clearly illustrates the existence of mode-specific IVR dynamics *i.e.*, differing nature of the IVR dynamics ensuing from CO stretch and the DCO bend bright states. In addition the role of the weak Fermi resonance involving the CO stretch and DCO bend modes is investigated. A key feature of the present work is that the techniques utilized for the analysis *i.e.*, parametric variations and local frequency analysis are not limited by the dimensionality of the system. This study, thus, explores the potential for understanding IVR in larger molecules from both time domain and frequency domain perspectives.

I. INTRODUCTION

Substantial progress has been made over the past few decades in understanding the nature of energy flow in highly excited molecules^{1,2,3,4,5,6,7,8}. At higher levels of excitation the usual rigid rotor-normal mode description breaks down and the modes get strongly coupled. The resulting spectral complexity in terms of the splittings and intensities encode the flow of energy through the molecule. This phenomenon of intramolecular vibrational energy redistribution (IVR) can lead to subtle but important deviations from the predictions of statistical theories like RRKM¹⁰ and thus profound consequences for the rates of chemical reactions⁹. The mode mixings in general have classical as well as quantum origins. Much of the classical effects arise from vibrational anharmonicities, coriolis and centrifugal distortion effects. Possible quantum contributions^{11,12,13,14,15,16} manifest as indirect state-to-state explorations involving a sequence of intermediate, off-resonance virtual states (“vibrational superexchange”). In molecules with symmetry the phenomenon of dynamical tunneling provides a quantum route to mode mixing^{14,15,16}. Theoretically it is crucial to establish and understand IVR pathways from time dependent as well as time independent perspectives. RRKM theory has been quite successful¹⁰ but evidence is mounting for a number of reactions where the intramolecular dynamics is inherently nonstatistical^{9,10}. Accounting for such nonstatistical dynamics is theoretically challenging and crucial for control of reactions.

In this work our aim is to understand IVR in the deuterated formyl radical DCO. Our choice of the system is primarily due to the considerable experimental¹⁷ and theoretical^{18,19,20,21} work on IVR and mode specificity of the unimolecular decay of highly vibrationally excited

DCO. In contrast to HCO the deuterated analog involves a strong accidental 1 : 1 : 2 resonance between the vibrational frequencies. The experiments and analysis of Renth *et al* using a effective Hamiltonian clearly shows that the unimolecular decay in DCO is IVR limited²⁰. Although DCO has three vibrational modes, m (DC stretch), n (CO stretch), b (bend), the coupling structure of the effective Hamiltonian²² yields a conserved quantity called as the polyad number $P = m + n + b/2$. Experimentally the existence of P is revealed by bunching of vibrational levels as evident in the SEP spectrum of DCO¹⁷.

As a small molecule exhibiting nonstatistical intramolecular dynamics DCO provides an ideal system to test the various theoretical approaches for studying highly excited molecules. Impressive advances have been made towards fully quantum investigation of the IVR dynamics in large systems^{7,9,23,24,25}. There is little doubt that DCO can be subjected to such exact treatments which are important in their own right. However there are strong reasons²⁶ to believe that powerful insights into IVR can be gained by approaches based on classical-quantum correspondence. For example, Jung *et al* have provided dynamical assignments of the highly excited states of DCO based on certain key periodic orbits in phase space²¹. A key to the success of the many classical-quantum correspondence studies^{26,27,28,29,30,31,32,33,34,35,36} is that the understanding of IVR is firmly rooted in the invariant structures inhabiting the underlying phase space. This provides a very clear dynamical picture of IVR in molecules and can serve as a baseline for estimating the important quantum routes to mode mixings.

Currently one of the main obstacles in extending such useful classical-quantum correspondence studies is the issue of dimensionality. Despite the existence of potentially

$3N - 6$ coupled vibrational modes it is now well understood that not all of the modes are coupled strongly^{7,9}. Although such hierarchicality of the couplings leads to much smaller dimensionalities of the ‘IVR space’ it is possible that for large enough molecules or smaller molecules at higher levels of excitation the effective dimensionality of the system can be larger than three. In such instances the dimensionality of the system poses both technical as well as conceptual problems in the context of classical-quantum correspondence studies. The technical problems are well known and have to do with the inability to visualize Poincaré surface of sections or the quantum states and, computation of the periodic orbits or higher dimensional tori. Thus the knowledge of the global phase space structure along with its influence on the quantum states is at present difficult to obtain for systems with three or more degrees of freedom. For more detailed discussions on the dimensionality issues, technical and conceptual, we refer the reader to the earlier works^{29,37,38,39,40}.

One of the central goals of our research is to come up with techniques that would allow a detailed classical-quantum correspondence study of IVR in molecules with three or greater degrees of freedom and in this context two approaches will be of particular interest. The first one is the promising technique of local frequency analysis (LFA) put forward nearly two decades ago by Martens, Davis and Ezra⁴¹. In their pioneering work^{41,42,43,44} on energy flow in the OCS molecule it was shown that LFA was capable of highlighting the role of various phase space structures including partial barriers and resonance zones. The important point is that although motion may be irregular when viewed over long time scales (several picoseconds), quantities such as frequencies can be constant over times corresponding to many vibrational periods. This gives rise to long time correlations and the notion of dynamically significant phase space regions^{41,42}. Since then very little work has been done in utilizing this technique for studying energy transport in multimode molecules. Interestingly much more efforts have been made in celestial mechanics⁴⁵ with fewer applications in atomic physics⁴⁶ and molecular systems⁴⁸. Recently Arevalo and Wiggins^{47,49} have proposed a technique for performing time-frequency analysis (LFA) which include strongly chaotic trajectories as well by using wavelet analysis. Applications to various systems demonstrated the advantages of a wavelet based LFA in understanding phase space transport⁴⁹.

A second technique⁵⁰ for analyzing the quantum states, based on parametric variations, was recently proposed by us and applied to a 2-mode model Hamiltonian. It was shown that variations of the eigenvalues with appropriate parameters *i.e.*, level velocities were strongly correlated to the important classical phase space structures organizing the quantum states. In the case of mixed and near-integrable systems the magnitudes and relative signs of the level velocities clearly indicated⁵⁰ the dynamical region of phase space associated with a given eigen-

state thereby providing a dynamical assignment of the states. The technique based on parametric variations is dimensionality independent, like the local frequency analysis mentioned before, and more importantly basis invariance is guaranteed. Moreover parametric variations can be used to identify localization, resulting in deviations from random matrix theory (RMT) predictions, even in strongly chaotic systems⁵¹. The full utility of parametric techniques is yet to be explored, particularly in the context of IVR⁵², and there do exist detailed semiclassical theories in the (near)integrable⁵³ and chaotic situations⁵¹.

Our system of choice DCO is effectively two dimensional due to the existence of the polyad P . Thus the intramolecular dynamics can be investigated in great detail using the existing methods. However DCO provides a stringent test for the dimensionality independent techniques mentioned above since there is significant chaos in the classical phase space for the lowest energies in $P = 3$ and 4. This paper is organized as follows: In section II the main features of the effective Hamiltonian and its classical limit are presented. This is followed, in section III, by a dynamical assignment of states in $P = 3, 4$ using the level velocities. It will be shown that a dynamical assignment based on level velocities, in conjunction with the inverse participation ratios⁵⁴ (IPR), can be given despite the presence of significant chaos. In section IV the time dependent dynamics of DCO are analyzed using local frequency analysis. This reveals the global picture of phase space transport and highlights chaotic trajectories undergoing rapid frequency jumps mainly between the stretch-stretch 1 : 1 resonance and the DC stretch-bend 2 : 1 Fermi resonance. Moreover it is seen that chaotic trajectories can be trapped in resonances for many vibrational periods. This is related⁵⁵ to the ‘stickiness’ of the chaotic trajectories and is of importance to the IVR dynamics in the molecule. The local frequency analysis also highlights the nature of the CO stretch-bend 2 : 1 Fermi resonance which is seen to play a role in the IVR for short times. Section V concludes.

II. EFFECTIVE HAMILTONIAN FOR DCO

The spectroscopic Hamiltonian, proposed recently by Tröllsch and Temps²², was obtained through a fit to the experimental DF and SEP spectra. The relevant matrix

elements are

$$H_{mnb;mnb} = \sum_j \omega_j \left(j + \frac{1}{2} \right) \quad (1a)$$

$$+ \sum_{jk} x_{jk} \left(j + \frac{1}{2} \right) \left(k + \frac{1}{2} \right)$$

$$H_{mnb;m-1,n+1,b} = \frac{\lambda_1}{2} (m(n+1))^{1/2} \quad (1b)$$

$$\times \left[1 + \lambda'_1 m + \lambda''_1 (n+1) + \lambda'''_1 \left(b + \frac{1}{2} \right) \right]$$

$$H_{mnb;m-2,n+2,b} = \frac{\lambda_2}{2} [m(m-1)(n+1)(n+2)]^{1/2} \quad (1c)$$

$$H_{mnb;m-1,n,b+2} = \frac{k_{mbb}}{2} \left[\frac{1}{2} m(b+1)(b+2) \right]^{1/2} \quad (1d)$$

$$H_{mnb;m,n-1,b+2} = \frac{k_{nbb}}{2} \left[\frac{1}{2} n(b+1)(b+2) \right]^{1/2} \quad (1e)$$

with $j = m, n, b$ denoting the zeroth order DC stretch, the CO stretch, and the bend modes respectively. The coupling terms λ_1 and λ_2 represent a 1 : 1 and a Darling-Dennison 2 : 2 resonance between the stretch modes respectively. The Fermi resonant couplings $k_{m(n)bb}$ correspond to a 1 : 2 resonance between the DC (CO) stretch and the bend modes. The effective Hamiltonian \hat{H} commutes with the polyad $P_Q = m + n + b/2$ and hence block diagonal in P_Q . A given P_Q block has $(P_Q + 1)(P_Q + 2)/2$ states for integer polyads and the states are labelled as P_{Qj} in order of decreasing energy. Note that the above Hamiltonian is able to approximately reproduce the experimental DF spectra for polyad values upto $P_Q = 5$ since $P_Q = 6$ was the highest polyad considered in the fitting procedure. Consequently the current work focuses on the polyads $P_Q = 3, 4$ as examples. The techniques used for the analysis in this work are, however, applicable to higher polyads as well. In what follows we will adopt a shorthand notation for the two main resonances, 1 : 1 DC stretch-CO stretch and 1 : 2 DC stretch-DCO bend, denoting them as mn and mbb respectively.

The classical limit Hamiltonian can be obtained using the Heisenberg correspondence

$$\hat{a}_j^\dagger \leftrightarrow I_j^{1/2} e^{i\phi_j} \quad \hat{a}_j \leftrightarrow I_j^{1/2} e^{-i\phi_j} \quad (2)$$

between creation-annihilation operators and the action-angle variables. The resulting classical Hamiltonian is

$$H = \sum_j \omega_j I_j + \sum_{jk} x_{jk} I_j I_k \quad (3)$$

$$+ \Lambda_1 (I_m I_n)^{1/2} \cos(\phi_m - \phi_n) + \lambda_2 I_m I_n \cos(2\phi_m - 2\phi_n)$$

$$+ \frac{I_b}{\sqrt{2}} [k_{mbb} I_m^{1/2} \cos(\phi_m - 2\phi_b) + k_{nbb} I_n^{1/2} \cos(\phi_n - 2\phi_b)]$$

with $\Lambda_1 \equiv \lambda_1 [1 + \lambda'_1 I_m + \lambda''_1 I_n + \lambda'''_1 I_b]$. As expected the zeroth order Hamiltonian H_0 is a function of the actions alone and the various couplings manifest themselves as

anharmonic resonances. The quantum zero point energy E_0 has been subtracted from the classical Hamiltonian for consistency. The classical system is effectively a two degree of freedom system due to the existence of the conserved quantity $P_c = 2(I_m + I_n) + I_b$ which is the analog of the quantum polyad. As a result the classical dynamics can be studied in a four dimensional reduced phase space. The reduction can be obtained by performing a canonical transformation via the generating function:

$$F = (\phi_m - 2\phi_b) J_m + (\phi_n - 2\phi_b) J_n + \phi_b P_c \quad (4)$$

The new action-angle variables are related to the old ones, $J_m = I_m, J_n = I_n, P_c = 2(I_m + I_n) + I_b$, and $\psi_m = \phi_m - 2\phi_b, \psi_n = \phi_n - 2\phi_b, \theta = \phi_b$. The resulting Hamiltonian²¹ is independent of the angle variable θ which is conjugate to P_c and hence an effectively two-dimensional system.

It is possible to perform a Chirikov⁵⁶ analysis of the classical Hamiltonian and obtain a resonance template in the state space²⁹. However it is seen that in this case the Chirikov analysis, which is based on the zeroth order H_0 , is not very suitable. This is mainly due to the reduced bend anharmonicity of DCO. Despite this limitation useful qualitative information can be obtained regarding the approximate location of the resonance zones and overlaps. For instance, such an analysis predicts that the CO stretch-bend Fermi resonance (k_{nbb}) does not show up in the state space for most of the polyads. Thus one anticipates the IVR dynamics in DCO to be dominated by the stretch-stretch 1 : 1 and DC stretch-bend 2 : 1 Fermi resonances. This observation is in agreement with earlier works^{20,21}. In what follows we will show the resonance template as a guideline and the local frequency analysis of the dynamics establishes the significant deviations from the zeroth order picture due to strong couplings.

III. DYNAMICAL ASSIGNMENTS OF STATES IN $P = 3$ AND $P = 4$

Considerable work has been done in the last few years to understand and possibly assign highly excited states by invoking the classical-quantum correspondence principle²⁶. Every single method, without exception, is based on identifying a dominant classical phase space structure that organizes the eigenstates in a given energy range. Indeed as DCO is effectively two dimensional due to the existence of the polyad it is possible to use any one of the several techniques proposed in the literature. However our objective in this work is to use techniques that do not explicitly rely on determining the exact periodic orbits and/or visualizations of the phase space and wavefunctions. This is especially important for analyzing systems with more than two degrees of freedom.

One such method was recently proposed by us⁵⁰ and it is based on the method of parametric variations. In this approach the "level velocities" $\dot{x}_\alpha(\tau)$ associated with an eigenstate $|\alpha(\tau)\rangle$ are determined and analyzed. Thus if

the effective, spectroscopic, Hamiltonian has the general form $H = H_0 + \sum_j \tau_j V_j$ with V_j and τ_j denoting the various resonances and the corresponding coupling strengths, then the level velocity of a specific eigenstate associated with a coupling V_j is obtained as:

$$\dot{x}_\alpha(\tau_j) \equiv \frac{\partial E_\alpha(\tau)}{\partial \tau_j} = \langle \alpha | V_j | \alpha \rangle \quad (5)$$

$$= \sum_{\mathbf{n}, \mathbf{n}'} c_{\alpha \mathbf{n}}^* c_{\alpha \mathbf{n}'} V_{j; \mathbf{n} \mathbf{n}'} = 2 \sum_{P_j} \dot{x}_\alpha(\tau_j; P_j) \quad (6)$$

In the above equation \mathbf{n} is the zeroth-order basis and $c_{\alpha \mathbf{n}} = \langle \mathbf{n} | \alpha \rangle$. The level velocity of a state $|\alpha\rangle$ with respect to V_j can be written as a sum over the polyads P_j , corresponding to the resonant perturbation V_j , of the partial level velocities $\dot{x}_\alpha(\tau_j; P_j)$. In the integrable limit *i.e.*, with only V_j present it is easy to see that $\dot{x}_\alpha(\tau_j) = \dot{x}_\alpha(\tau_j; P_j)$. In the presence of other perturbations $V_{i \neq j}$ the level velocity $\dot{x}_\alpha(\tau_j)$ can have contributions from many different P_j indicating extensive mixing. Thus the level velocity essentially measures the response of the quantum eigenvalue to a specific perturbation.

It was established⁵⁰ in the earlier work that $\dot{x}_\alpha(\tau_j)$ is correlated to the phase space nature of the eigenstate. For integrable, single resonance cases the various properties of the level velocities are well known⁵⁷. In the case of mixed phase space systems it is still possible⁵⁰ to dynamically assign states based on the level velocities since the regular regions strongly influence the eigenstates. In case of near integrable systems and, to some extent, for mixed systems the correlation of the level velocities with the phase space can be understood semiclassically since it is possible to write⁵⁰

$$\dot{x}_\alpha(\tau_j) = \text{Tr}[\hat{V}_j |\alpha\rangle \langle \alpha|] \quad (7)$$

$$\approx \frac{1}{(2\pi\hbar)^N} \int d\mathbf{I} d\boldsymbol{\theta} V_j^W(\mathbf{I}, \boldsymbol{\theta}) W_\alpha(\mathbf{I}, \boldsymbol{\theta}) \quad (8)$$

where V_j^W is the Weyl symbol of the operator \hat{V}_j and W_α is the Wigner function associated with the eigenstate $|\alpha\rangle$. For near integrable systems the Wigner function condenses on to the invariant torus⁵⁸ thus explaining the observed correlation.

However for systems with considerable chaos it is not *a priori* clear whether the correlation continues to hold. The $P = 3, 4$ cases for DCO considered herein show extensive chaos at low energies and hence provide a critical test for the level velocity approach. In the extreme limit of an ergodic system the Berry-Voros hypothesis states that^{58,59,60}

$$W_\alpha(\mathbf{I}, \boldsymbol{\theta}) = C \delta[E_\alpha - H(\mathbf{I}, \boldsymbol{\theta})] \quad (9)$$

In this limit it is easy to see that \dot{x}_α is essentially the parametric derivative of the smooth part of the spectral staircase function⁶⁰. This term is independent of the nature of the dynamics and in particular refers to contributions from short time orbits. Nevertheless it is well known

that even in strongly chaotic systems the periodic orbits (unstable) play a crucial role⁶¹. Thus it is expected that in such systems the level velocities are influenced by the periodic orbits. A more general expectation is that, independent of the nature of the dynamics, closed orbits will influence the level velocities. As the purpose of the current work is not to provide a semiclassical expression for computing the level velocities, we will briefly outline the reasons for such an expectation. The arguments provided are not new and appear in an early work by Eckhardt *et al.* where semiclassical matrix elements were determined from periodic orbits⁶². To begin with define a quantity

$$g_{V_j}(E) = \text{Tr} \hat{G} \hat{V}_j \quad (10)$$

with \hat{G} being the energy Green's function and \hat{V}_j is the perturbation of interest. Using the formal definition of \hat{G} it is straightforward to show that

$$\rho_{V_j}(E) \equiv -\frac{1}{\pi} \text{Im} g_{V_j}(E) = \sum_{\alpha} \dot{x}_\alpha(\tau_j) \delta(E - E_\alpha) \quad (11)$$

Thus $\rho_{V_j}(E)$ has poles at the eigenvalues E_α and the residues are precisely the level velocities $\dot{x}_\alpha(\tau_j)$. The quantity $g_{V_j}(E)$ can be written in the semiclassical limit as:

$$g_{V_j}(E) = \int d\mathbf{I} d\boldsymbol{\theta} V_j^W(\mathbf{I}, \boldsymbol{\theta}) G_W(\mathbf{I}, \boldsymbol{\theta}; E) \quad (12)$$

with G_W being the Wigner transform of the Green's function. The above integral can be evaluated via stationary phase approximation and, apart from the smooth short time contribution, gives rise to an oscillating term. The oscillating part can be evaluated for integrable (Berry-Tabor)⁶³, near-integrable (Almeida-Ullmo-Grinberg-Tomsovic)⁶⁴, and chaotic (Gutzwiller)⁶⁵ cases. In every case the oscillating part depends on the stabilities of the closed orbits and involves the classical time average of V_j over the period of the closed orbits⁶⁶. Since the level velocities are extracted as residues of the oscillating part it is reasonable to expect a strong influence of the closed orbits and their stabilities. Note that extracting the velocities from this approach is rather involved. Since it is difficult to obtain bounds on the velocities using semiclassical techniques in the mixed phase space case and the effect of various bifurcations on the level velocities is not known as of yet we will explore the utility of the technique in dynamical assignments from a qualitative perspective. The basis for the assignments will be explicitly discussed for the case $P = 3$ since the arguments are fairly general.

In table I we show the states in polyad $P = 3$, the level velocities with respect to the mn and the mbb resonances and the IPR in three different basis. We start by noting that the maximum integrable limit velocities expected (appendix of Ref. 50) are 1.5 and 2.8 for the $\dot{x}_{\alpha, mn}$ and $\dot{x}_{\alpha, mbb}$ respectively. Moreover since the coupling constants $\lambda_1, k_{mbb} > 0$ it is also anticipated, based

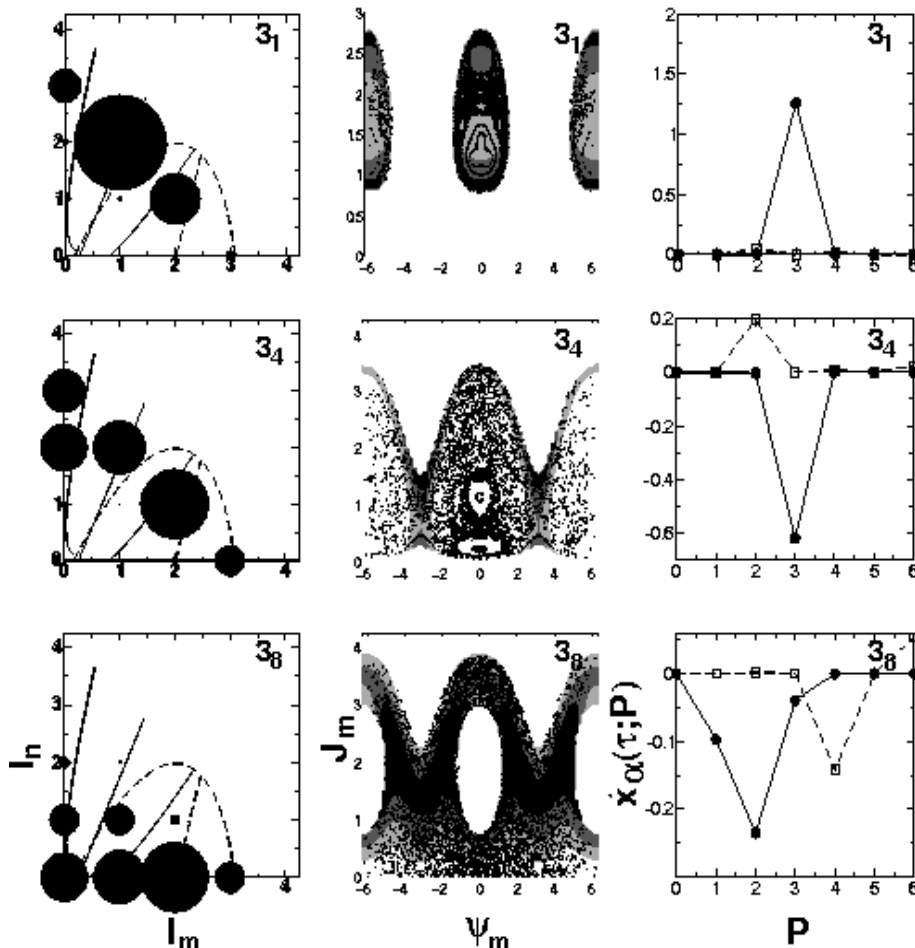


FIG. 1: State space representation (left panels), Husimi distributions superposed on the surface of section (middle panel), and partial level velocities (right panels) are shown for selected states in $P = 3$. The resonance zones computed using Chirikov approximation are also shown in the state space. The mn zone is shown as solid lines and the mbb zone is shown as the dashed lines. Three contours of the Husimis are shown for clarity. The states shown are 3_1 (top row), 3_4 (middle row), and 3_8 (bottom row). Note that the Husimis of states 3_1 and 3_4 are localized around the stable and unstable regions of the classical phase space. The Husimi of state 3_8 is delocalized over the surface of section and the partial velocity data indicates strong mixing. The maximum contour value for 3_8 is one third of the maximum value for state 3_1 .

on the earlier work⁵⁰, that large positive velocities correspond to stable (elliptic) regions of the phase space and large negative velocities correspond to unstable (hyperbolic) regions of the phase space. Consequently the highest energy state 3_1 is clearly a mn state with the corresponding Husimi localized around a stable region of the phase space. The high IPR in the mn basis and the small level velocity with respect to the mbb resonance clearly support such an assignment. Thus we expect state 3_1 to be localized in the state space as well and associate an approximate integrable limit polyad P_{mn} with the state. Our expectations are confirmed and Fig.1 shows the state space representation of 3_1 and the corresponding Husimi superposed on the surface of section. The approximate polyad P_{mn} can be extracted by looking at the partial level velocities, shown in Fig.1, and one obtains $P_{mn} = 3$. The state 3_2 has comparable positive velocities both with

respect to mn and mbb *i.e.*, $\dot{x}_{mn}(3_2) \approx \dot{x}_{mbb}(3_2)$. This suggests that the state is influenced by both the resonances and confirmed by inspecting the state space representation of the state as well as the partial velocities. However since the IPR $L_{mn}(3_2) > L_{mbb}(3_2)$ and the integrable limit mn velocity is expected to be small for this state, 3_2 is assigned as a mn state with $P_{mn} = 3$. The next state 3_3 can be clearly assigned based on the (partial) level velocities as well as the IPRs as a mn state localized about a stable periodic orbit with $P_{mn} = 2$. State 3_4 has a negative mn velocity with large IPR in the mn basis and hence it is expected to be located in the unstable region of the phase space. The Husimi of the state shows a typical separatrix-like structure (cf. Fig.1) and hence agrees with the velocity analysis. Based on the partial velocity data it is straightforward to assign an approximate $P_{mn} = 3$ for 3_4 . Analogous to the state

TABLE I: Dynamical assignments for states in $P = 3$

State	E (cm ⁻¹)	\dot{x}_{mn}	\dot{x}_{mbb}	L_0	L_{mn}	L_{mbb}	Assignment ^a
3 ₁₀	4885	-0.09	-1.81	0.55	0.56	0.91	P_{mbb}, u
3 ₉	4935	-0.55	-0.40	0.65	0.80	0.78	dl
3 ₈	5032	-0.37	-0.09	0.24	0.33	0.70	mbb
3 ₇	5138	-0.11	0.45	0.51	0.29	0.46	$*, P_{mbb}$
3 ₆	5177	-0.02	1.09	0.34	0.33	0.41	$*, P_{mbb}^b, s$
3 ₅	5289	-0.31	0.09	0.33	0.60	0.39	$P_{mn} - 1$
3 ₄	5354	-0.62	0.23	0.25	0.69	0.22	P_{mn}, u
3 ₃	5415	0.60	0.13	0.41	0.71	0.34	$P_{mn} - 1, s$
3 ₂	5469	0.22	0.23	0.46	0.81	0.49	P_{mn}, nom
3 ₁	5644	1.26	0.07	0.54	0.99	0.53	P_{mn}^c, s

^a s, u and dl stand for stable, unstable and distorted local respectively. The approximate polyads $P_{mn} = m+n$ and $P_{mbb} = 2m+b$. States involved in avoided crossings are denoted by $*$.

^bThe value of $P_{mbb} = 6$ is deduced from the partial velocity data.

^cThe value of $P_{mn} = 3$ is deduced from the partial velocity data. See Fig. 1

3₂ it is possible to nominally assign the state 3₅ as a mn state with $P_{mn} = 2$. State 3₁₀ has a large negative \dot{x}_{mbb} and can be clearly associated with the unstable region in phase space with $P_{mbb} = 6$. Again, inspection of the Husimi and the partial velocities supports the assignment.

We now discuss states that are either difficult to assign or unassignable. The particularly strong mixings in these states can arise due to avoided crossings and/or strong overlap of the various resonances zones. The notoriety of multistate avoided crossings in the process of assignments are well known and one expects them in sufficiently non-integrable systems. State 3₆ has a large positive mbb velocity and is expected to be an mbb state localized about a stable periodic orbit. However the velocity is about half of the maximum expected in the integrable limit and the IPRs are about the same in all three basis. The partial velocities clearly show that 3₆ can be assigned as a mbb state with $P_{mbb} = 6$. The state 3₇ is an interesting state since the IPR in the zeroth order basis is larger than the IPRs in either the mn or the mbb basis. Indeed the state space picture and the Husimis of the state 3₇ rule out a clear mn or mbb assignment. A closer inspection reveals that the states 3₆ and 3₇ are involved in an avoided crossing with respect to both λ_1 and k_{mbb} . This explains the observed lower than maximum velocity of the state 3₆. This quantum mixing, seen in earlier studies^{21,30}, is clearly 2-state and it is possible to demix the states yielding states $|\alpha(\beta)\rangle = |3_6\rangle \pm |3_7\rangle$ and analyze the velocities. On demixing it is found that $\dot{x}_{mbb}(\alpha) = 2.2$ which is closer to the maximum value expected for an mbb state in polyad $P = 3$. The other velocities indicate dominance of the mbb coupling and $\dot{x}_{mbb}(\beta) = -0.65$ thus leading to an assignment of the state 3₇ as mbb with $P_{mbb} = 4$.

State 3₈ is a typical example of a difficult state to assign. In Fig.1 the state space representation, Husimi,

TABLE II: Dynamical assignments for states in $P = 4$

State	E (cm ⁻¹)	\dot{x}_{mn}	\dot{x}_{mbb}	L_0	L_{mn}	L_{mbb}	Assignment ^a
4 ₁₅	6167	-0.67	-0.31	0.80	0.95	0.84	dl
4 ₁₄	6392	-0.30	-3.38	0.22	0.25	0.76	P_{mbb}, u
4 ₁₃	6448	-0.30	-0.98	0.36	0.40	0.76	P_{mbb}
4 ₁₂	6593	-0.30	0.83	0.22	0.27	0.81	P_{mbb}
4 ₁₁	6715	0.07	-1.35	0.54	0.50	0.68	$P_{mbb} - 2, u$
4 ₁₀	6773	-0.28	3.35	0.32	0.32	0.72	P_{mbb}, s
4 ₉	6809	-0.59	-0.47	0.38	0.70	0.47	dl
4 ₈	6875	-0.37	0.13	0.13	0.29	0.34	$mixed$
4 ₇	6965	0.15	0.09	0.47	0.30	0.35	$*, P_{mn} - 2$
4 ₆	7017	-0.08	1.18	0.30	0.27	0.27	$*, P_{mbb} - 2, s$
4 ₅	7101	-0.01	0.32	0.36	0.57	0.40	$mixed$
4 ₄	7168	-0.81	0.19	0.27	0.78	0.26	P_{mn}, u
4 ₃	7241	1.03	-0.06	0.33	0.61	0.41	$P_{mn} - 1, s$
4 ₂	7287	0.64	0.41	0.23	0.65	0.29	P_{mn}
4 ₁	7470	1.81	0.07	0.49	0.99	0.47	P_{mn}, s

^aThe notations are same as in table I. The values $P_{mn} = 4, P_{mbb} = 8$ are deduced from the partial velocity data. See Fig. 2.

and the partial velocity data is shown for 3₈. The velocity data indicates this to be a mn state whereas the IPR data supports a mbb assignment. Note that this state has the lowest IPR in the zeroth order basis amongst the set of states in $P = 3$. The particularly high value of the IPR in the mbb basis suggests that it is quite possible for this state to have a small velocity even in the single, mbb only integrable case. Indeed on computing the integrable limit one obtains $\dot{x}_{mbb}(3_8) \approx -0.13$. Thus it is possible to assign the state 3₈ as a mbb state. Note that the partial velocity data suggests $P_{mn} = 4$ but the state space representation exhibits $P_{mbb} = 6$. The difficulty, in part, arises from the fact that it is quite possible for a state to have a velocity close to zero and yet be strongly influenced by that resonance⁵⁷. A similar situation arises for the state 3₉ in that the level velocities are very similar. In this case, however, the IPRs are very similar and high in all three basis. This is a typical signature of a distorted local mode state. In this instance the state is influenced slightly by both the resonances leading to the similar velocities and IPRs.

The states for $P = 4$ can be assigned in a similar fashion and the assignments are shown in table II. In particular, all the states except 4₈ and 4₅ can be assigned in analogy with the states in $P = 3$. Thus the states 4₈ and 4₅ are classified as mixed. In Fig.2 states with large positive (4₁₀) and large negative (4₁₄) mbb velocities are shown. Note the localization of the Husimis in the stable and unstable regions of the phase space. The state space, Husimi and partial velocity data for the mixed state 4₈ are shown in Fig.2 as an example. Extensive delocalization is seen for this state in both the state space and the phase space. The state 4₈ also happens to have the lowest IPR among the states in $P = 4$. We note that for

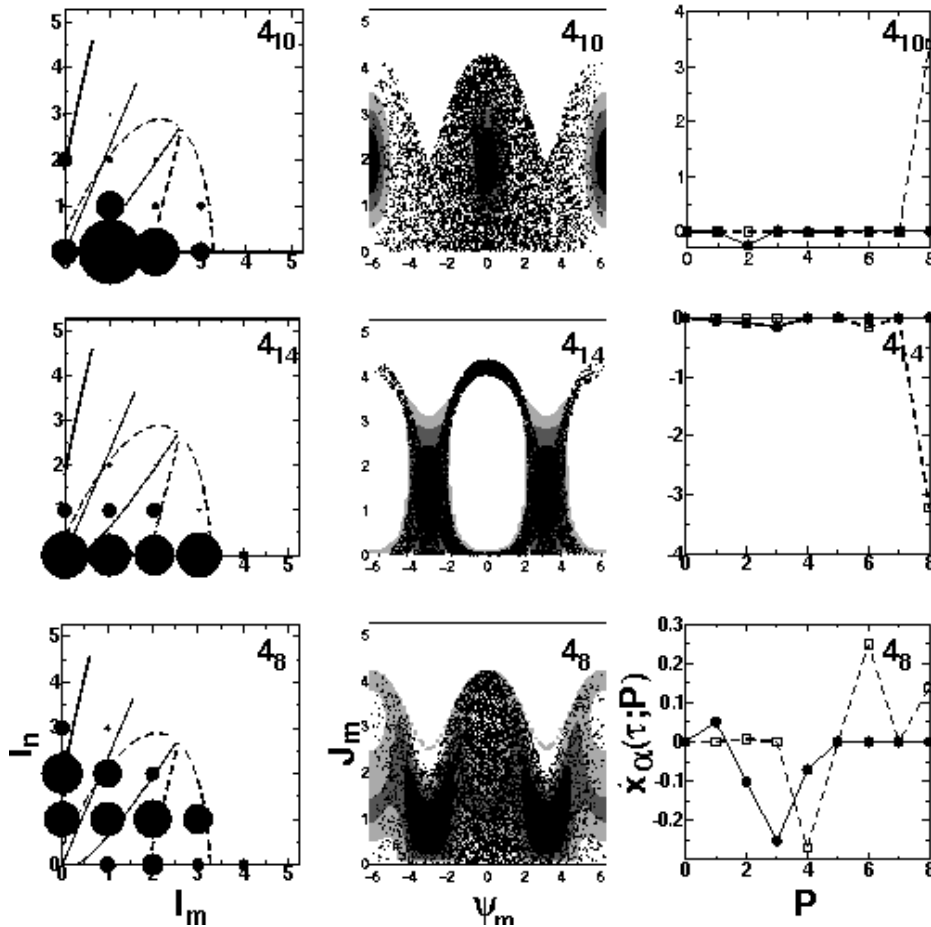


FIG. 2: Same as in Fig. (1) for three states in $P = 4$. The states shown are 4_{10} (top row), 4_{14} (middle row), and 4_8 (bottom row). Note that the Husimis of states 4_{10} and 4_{14} are localized around the stable and unstable regions of the classical phase space. The Husimi of state 4_8 is delocalized over the surface of section and the partial velocity data indicates strong mixing.

$P = 4$ the maximum expected velocities for the mn and the mbb are 2.0 and 4.4 respectively.

A general observation regarding the assignments is that the lower energy states of the polyads are dominated by mbb whereas the higher end states are influenced more by the mn resonance. States in the middle of the energy regions exhibit transitional character. Similar observations were made in the dynamical assignments of the states in $P = 8$ by Jung *et al*²¹. Note that the assignments made in this work are essentially based on the level velocities and the IPRs. Thus our assignment does not invoke any explicit quantum numbers based on periodic orbits. However it is clear that attaching an approximate polyad and noting the signs on the level velocities is providing dynamical information. For instance state 4_1 having a large $\dot{x}_{mn} > 0$ implies that the state is influenced by a stable periodic orbit of the mn type. In particular this state would be considered as a C class state with the assignment ($l = 4, t = 0$) in the notation of the previous work²¹. The approximate polyad P_{mn} can be identified with the longitudinal quantum number

l . A crucial point regarding the assignments using level velocities is worth reiterating at this juncture. The advantage of using the level velocities is based on strong correlation of the velocities with the phase space nature of the eigenstates. Such dynamical informations cannot be obtained by using the IPRs alone or the various representations of the eigenstates. For example, in $P = 3$ the IPRs $L_{mn}(3_3) \approx L_{mn}(3_4)$ and one would correctly infer that both states are of mn type. However with $\dot{x}_{mn}(3_4) \approx -\dot{x}_{mn}(3_3)$ it is possible to provide a finer distinction between the two states ; 3_3 is associated with a stable region of the phase space whereas 3_4 is located in the unstable region of the phase space.

IV. LOCAL FREQUENCY ANALYSIS: PHASE SPACE DIFFUSION AND TRANSPORT

As mentioned before the Chirikov analysis of DCO resonances based on the zeroth order classical $H_0(\mathbf{I})$ is not very accurate due to strong resonant couplings of the

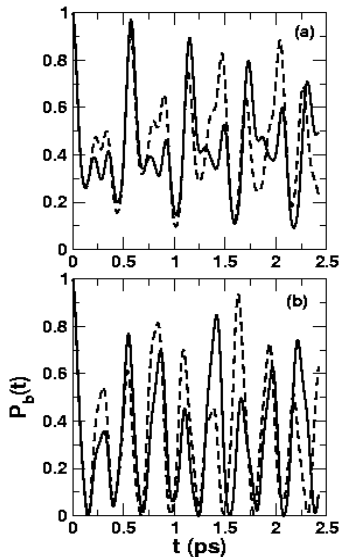


FIG. 3: Survival probabilities for the ZOBS (a) $|030\rangle$ and (b) $|040\rangle$. Solid line is the exact Hamiltonian and dashed lines are with $k_{nbb} = 0$.

various modes. The surface of sections indicate that for polyads $P = 3, 4$ there is considerable stochasticity even at the lowest energy. This implies that the various resonances overlap strongly for these polyads and most trajectories are chaotic. Despite the significant amount of chaos in the phase space the Husimis of many eigenstates were seen to be rather localized. Such observations have been made earlier in other studies and it is well known that a largely chaotic phase space can still contain structures that act as partial barriers to phase space transport. The partial barriers can arise due to cantori as well as broken seperatrices and existence of such structures can lead to eigenstate localization. Moreover even in the case of strongly chaotic systems eigenstates can get scarred by periodic orbits leading to localization. In recent years it has been understood that such partial barriers and periodic orbit scarring lead to statistically significant deviations from the predictions of RMT. Infact the level velocities, studied in the previous section, already encode such localization information. From the IVR perspective, several studies^{7,9} have now established that the energy flow process is hierarchical and that a hierarchical local random matrix (HLRM) approach is more appropriate to understand IVR. The important factor is the local density of coupled states and not the total density of states at a given energy which leads, amongst other observations, to a power law decay of the survival probability on intermediate timescales⁶⁷.

Based on the detailed work on classical phase space transport⁶⁸ it is tempting to conjecture that the hierarchical nature of IVR is intimately connected to the various partial barriers in the phase space. The important work^{41,42} by Davis and Martens *et al* on OCS seems to support the conjecture. However, except for

earlier works on OCS, there have not been many efforts to identify partial barriers for transport in the context of IVR in molecules. The importance of such an undertaking lies in the fact that it might prove crucial in controlling IVR as well. In DCO it has been established that the unimolecular decay is IVR limited^{17,20}. Moreover, previous studies^{18,20,21} on DCO suggest that the Fermi resonance between the CO stretch and DCO bend is unimportant. The approximate Chirikov analysis also indicates the muted role of the *nbb* Fermi resonance. In Fig.3 the survival probabilities for the zeroth order bright states $|030\rangle$ and $|040\rangle$ in the absence of the *nbb* Fermi resonance are shown and compared to the full system. It is clear from the figure that although the initial decay from the bright states is controlled by the 1 : 1 (for about 100 fs) the *nbb* Fermi resonance starts to play a role around 200 fs. Is it the case that the *nbb* resonance does play a role, albeit in a secondary fashion, in the short time tier structure? Why is the initial decay from $|040\rangle$ apparently complete by about 150 fs as opposed to those of $|030\rangle$ and $|050\rangle$? In other words what makes the 1 : 1 so effective for the bright state $|040\rangle$? The answers to these questions are not straightforward and in this work we will try to provide some approximate answers. We believe that the LFA technique is capable of addressing some of these crucial issues. Ahead a brief introduction is given to the technique of LFA and we refer the reader to the work by Martens *et al*⁴¹ and Arevalo *et al*^{47,49} for more details.

The classical limit of the spectroscopic Hamiltonians are nonlinear, multiresonant Hamiltonians which are functions of the zeroth order actions \mathbf{I} and the angles ϕ . The classical limit Hamiltonians have a typical form $H(\mathbf{I}, \phi) = H_0(\mathbf{I}) + \sum_j V_j(\mathbf{I}, \phi)$ where the various resonant perturbations are denoted by V_j . In the absence of the perturbations the system is described by H_0 which is classically integrable. In such cases the various nonlinear frequencies $\Omega(\mathbf{I}) = \partial H_0 / \partial \mathbf{I}$ are time-independent and one can define a frequency map $\mathbf{I} \rightarrow \Omega(\mathbf{I})$ which, if invertible, can be used to characterize the phase space. The frequency map can be used to characterize the phase space, thanks to the KAM theorem, for near-integrable systems as well. For a system like DCO there are three frequencies $\Omega \equiv (\Omega_m, \Omega_n, \Omega_b)$ and it is useful to visualize the dynamics in the frequency ratio space. However for non-quasiperiodic trajectories, associated with the full nonintegrable Hamiltonian, the various frequencies $\Omega(\mathbf{I})$ vary with time since increasing perturbation strengths lead to the breakdown of KAM tori and widespread chaos. Despite the time dependence of the frequencies it has been observed in many systems that the frequencies can remain approximately constant over times corresponding to many vibrational periods. Thus even non-quasiperiodic trajectories can spend an appreciable amount of time in one part of the phase space before passing on to another region of the phase space. This in turn implies existence of long time correlations and gives rise to the concept of dynamically significant regions of phase space. The

concept of local frequencies *i.e.*, time-varying frequencies allows one to identify such dynamically significant regions of phase space.

Two main approaches are available to extract the local frequencies from a classical trajectory. The first one proposed by Martens *et al*⁴¹, and a similar one by Laskar⁴⁵, uses Fourier transforms of short time segments of long trajectories. We are interested in the more recent work^{47,49} by Arevalo and Wiggins wherein the local frequencies are obtained by a continuous wavelet transform of the trajectories. In this approach a general time dependent function $f(t)$ is expressed in terms of the basis functions constructed as translations and dilations of a mother wavelet⁶⁹

$$\psi_{a,b}(t) = a^{-1/2}\psi\left(\frac{t-b}{a}\right) \quad (13)$$

The coefficients of this expansion are given by the wavelet transform of $f(t)$, defined as

$$L_\psi f(a,b) = a^{-1/2} \int_{-\infty}^{\infty} f(t)\psi^*\left(\frac{t-b}{a}\right) dt \quad (14)$$

for $a > 0$ and b real. The wavelet transform gives the local frequency of $f(t)$ over a small interval of time around $t = b$ and inverse of the scale factor a is proportional to the frequency. A distinct advantage of the wavelet approach is that the time window automatically narrows for high frequency and widens for low frequency. The value of the local frequency at a given time $t = b$ is extracted⁴⁷ by determining the scale a which maximizes the modulus of the wavelet transform. Throughout this work, as in Arevalo and Wiggins, we will use the Morlet-Grossman mother wavelet

$$\psi(t) = \frac{1}{\sigma\sqrt{2\pi}} e^{2\pi i\lambda t} e^{-t^2/2\sigma^2} \quad (15)$$

with $\lambda = 1$ and $\sigma = 2$. The parameters λ, σ can be tuned to improve the resolution. Within the wavelet approach the local frequencies can be obtained even for chaotic trajectories. For a strongly chaotic trajectory the frequencies will vary considerably and one can measure the “diffusion” of the k^{th} frequency by evaluating

$$d_k(T) = \frac{1}{T} \int_0^T dt |\Omega_k(t) - \bar{\Omega}| \quad (16)$$

where $\bar{\Omega}$ is the mean frequency and T is the total time to which the trajectory is propagated. This measure of diffusion characterizes the unstable regions of phase space and thus low diffusion implies either quasiperiodic motion or extensive trapping near resonance zones (see below). For our application to DCO we choose initial conditions for the trajectories in the following fashion. A uniform grid is chosen in the state (zeroth order action) space (I_m, I_n) with I_b being fixed by the polyad conservation. A particular choice of the angles (ϕ_m, ϕ_n, ϕ_b) then provides initial conditions corresponding to a specific slice

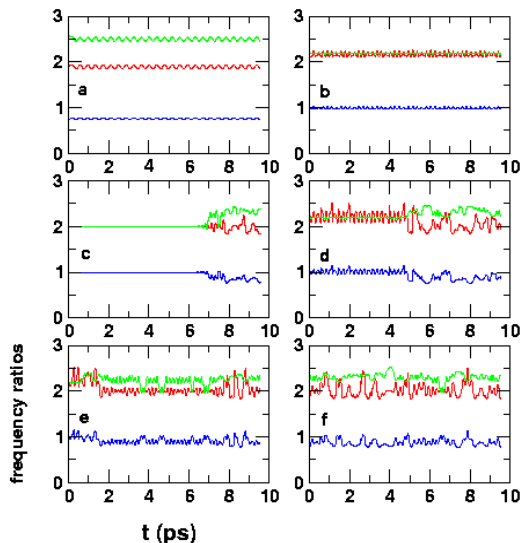


FIG. 4: The three frequency ratios for DCO for various trajectories at energy $E = 5145 \text{ cm}^{-1}$. Total time of propagation $T = 10$ ps. Ω_m/Ω_n is shown in blue, Ω_m/Ω_b is shown in red and Ω_n/Ω_b is in green. See text for details on each trajectory.

of the phase space. The numerically integrated trajectories over certain time interval $[0, T]$ are expressed as $z_k(t) = \sqrt{2I_k(t)}e^{i\phi_k(t)}$ for $k = m, n, b$. The three local frequencies $\Omega_k(t)$ are extracted by computing the maxima of the modulus of the wavelet transforms of $z_k(t)$ *i.e.*, $\max_a |L_\psi z_k(a, b)|$. Note that the maxima are obtained with a fractional precision of 10^{-8} . Details regarding the numerical procedure to extract the maxima can be found in the work of Arevalo *et al*⁴⁷.

A large number of trajectories for both $P = 3$ and $P = 4$ at various energies were analysed and many distinct dynamical behaviours were repeatedly seen. In Fig.4 we show, as examples of such dynamical patterns, six trajectories whose frequency ratios were computed to about $T = 10$ ps. Note that 10 ps is a fairly long time and corresponds to about 500 CO vibrational periods. All of the six trajectories are at an energy $E = 5145 \text{ cm}^{-1}$ which is energetically close to the middle of the polyad $P = 3$. The phase space structure is shown in Fig.5 for reference and one can clearly see large regions of stochasticity. Figure (a) shows a typical quasiperiodic, nonresonant trajectory which in this case represents a distorted local mode. The corresponding trajectory is shown in the surface of section (circles in Fig.5) as well. In Fig.4b a 1 : 1 resonant regular trajectory corresponding to the small island on the surface of section is shown. Notice the locking of the relevant frequency ratio *i.e.*, $\Omega_m/\Omega_n \approx 1$ for the entire duration. In Fig.4c a trajectory with initial conditions very close to a periodic orbit of the full system is shown. All the frequency ratios are locked perfectly for about 7 ps and later show large diffusion. Interestingly in this case the nbb locking $\Omega_n/\Omega_b = 2$

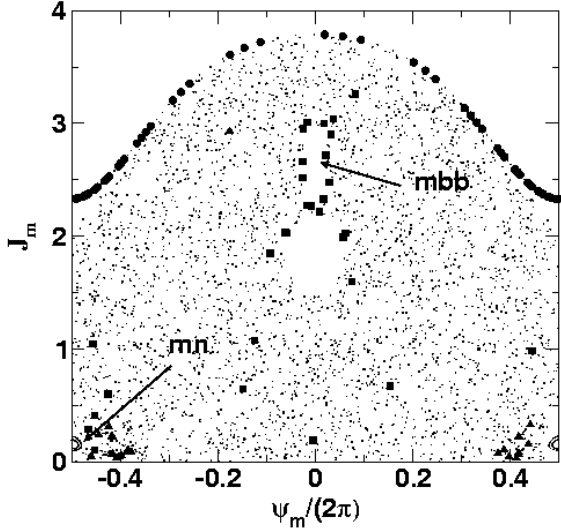


FIG. 5: Classical Poincaré surface of section at $E = 5145 \text{ cm}^{-1}$. The variables are $J_m = I_m$ and $\psi_m = \phi_m - 2\phi_b$. Selected trajectories (cf. Fig.4) are highlighted with filled circles (a), triangles (d), and squares (e). The highlighted trajectories are plotted for about 5 ps.

is clearly seen and thus any other initial condition close to this would certainly involve the nbb resonance to some extent. In Fig.4d we show an example of a trajectory exhibiting resonance trapping. This particular trajectory is trapped in the $1 : 1$ resonance for nearly 5 ps and then drifts away. The corresponding trajectory is plotted in the surface of section (triangles in Fig.5) and it is seen that this trapping is due to the stickiness of the small $1 : 1$ island. The trajectory is chaotic for longer times but the observed stickiness suggests that even tiny regions of regularity in the phase space can sufficiently influence the dynamics. Another example of a trapped trajectory is shown in Fig.4e with the corresponding behaviour on the surface of section shown in Fig.5 (squares). In this case the trajectory starts out with frequency locked in the $1 : 1$ but drifts away quickly and gets trapped into the $\Omega_m/\Omega_b \approx 2$ ratio for almost 6 ps. Finally in Fig.4f we show a typical chaotic trajectory with large diffusion and no apparent long time trapping in any of the fundamental resonances. Two points are worth reiterating in the context of the examples shown in Fig.4 and Fig.5. The first is that all these various, and other, dynamical behaviors are found at the same energy indicating the rich structure inherent to the classical phase space. This energy is by no means special and indeed similar observations hold for other energies in the polyad $P = 3$ as well as different polyads. Secondly, the overall phase space might look chaotic on long time scales but the regular regions, even those with phase space area $< \hbar$, lead to significant stickiness^{49,55} and hence long time trappings in one or the other significant resonance zone. This observation, we emphasize again, is not new and is well known in the

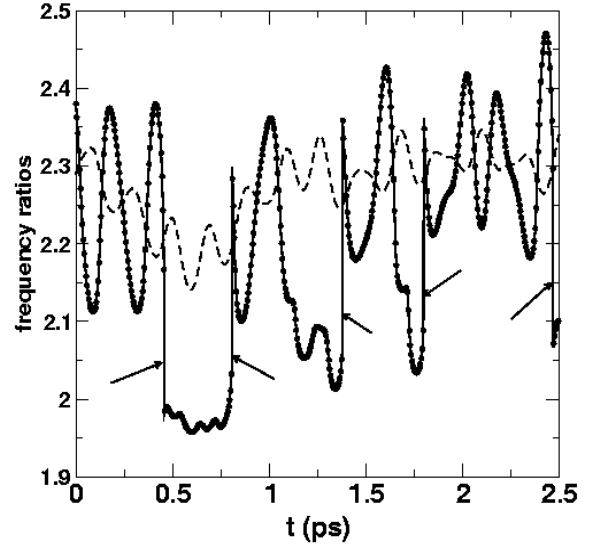


FIG. 6: A trajectory for $P = 4$ exhibiting rapid frequency jumps. For clarity the ratios Ω_m/Ω_b (solid line with points) and Ω_n/Ω_b (dashed) are shown. Note that the jumps (indicated by arrows) take the trajectory from being near mbb resonance to being near the mn resonance. Only a 2.5 ps portion of the 15 ps trajectory is shown. The jumps occur over the entire time span.

nonlinear dynamics community. However in this work we are demonstrating this effect for a realistic spectroscopic Hamiltonian with important consequences for IVR in the molecule.

A further dynamical effect that occurs in DCO has to do with rapid jumps in the frequency ratio space. An example for $P = 4$ is shown in the Fig.6 where the ratio Ω_m/Ω_b is undergoing rapid jumps between otherwise smooth variations. Note that the ratio Ω_n/Ω_b is fairly smooth and does not exhibit the rapid jumps. The jumps in the frequency ratio happen from the trajectory being near the mbb resonance to the trajectory being near the mn resonance. Such rapid jumps have been observed by Arevalo in OCS as well as the planar 3-body problem⁴⁹. In this instance the jumps seem to correspond to heteroclinic orbits that connect the mbb and the mn resonance zones. However confirming this involves computing invariant manifolds and their intersections which is far from easy. Nevertheless, such rapid resonance transitions could have important implications for the nature of IVR in DCO.

To indicate the strongly coupled nature of the DCO dynamics we show the total diffusion for $P = 4$ over the state space in Fig.7. In Fig.7a the diffusion is shown for the phase space slice $\phi_m = \phi_n = \phi_b = 0$. For reference Figs.7c,d show the diffusion data for integrable mn and mbb subsystems. It is easy to see the mn and mbb resonance zones in the integrable single resonance cases. Comparing to Fig.7a it is clear that the resonances have overlapped strongly. Further in Fig.7b we show the diffu-

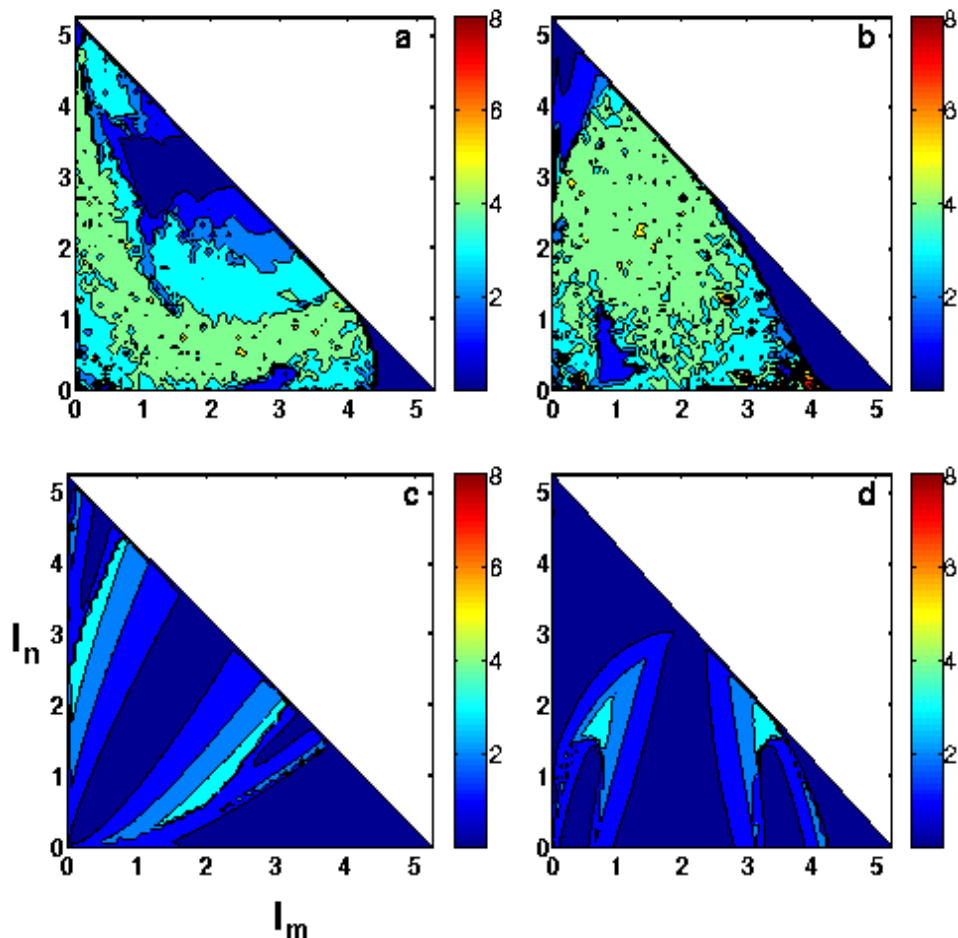


FIG. 7: Total diffusion (ps^{-1}) in the state space for $P = 4$ computed for $T = 10$ ps. In (a) and (b) the phase space slices are $(0, 0, 0)$ and $(0, \pi, 0)$ respectively. The integrable subsystems are shown for reference in (c) mn and (d) mbb respectively. In (c) and (d) the resonance zones can be seen clearly. In (a) and (d) there are no isolated resonances and the system is strongly coupled.

sion for the phase space slice $\phi_m = 0 = \phi_b, \phi_n = \pi$. Note that the diffusions for the two slices of phase space are dramatically different. This implies that it is not possible to understand the intramolecular dynamics of DCO based on H_0 alone. A key observation here is that the diffusions in state space show significant heterogeneity. For instance in Fig.7a,b we have regions of similar diffusion strengths separated by a region of larger diffusion strengths. Thus if one imagines going along a specific mn or mbb polyad in state space then alternating diffusion strengths are encountered. Similarly along a specific energy contour the diffusion values can vary considerably. This leads to trappings of the classical trajectory and hence bottlenecks to energy flow. For instance in Fig.7b the region of low diffusion around $(I_m, I_n) \approx (1.0, 0.5)$ is due to the existence of a periodic orbit of the full system. In the semiclassical limit the heterogeneous nature of the state space diffusion can have interesting consequences for eigenstate localizations.

Temps *et al.* discuss²⁰ the differences between choos-

ing a CO-stretch bright state (experimental) versus the DCO bend bright states. It was shown that the DCO bend states undergo much faster unimolecular decay. In order to gain dynamical insights into their findings the various bright states were analyzed from the LFA perspective. Several initial conditions corresponding to the bright states *i.e.*, $E = E_{ZOBs}$ were generated with the actions (I_m, I_n, I_b) corresponding to the bright state of interest and randomly choosing the angle (ϕ_m, ϕ_n, ϕ_b) variables. The various dynamical quantities of interest are then averaged over the angles. This is done for two main reasons. First, although the correspondence between actions and quantum numbers is well known a similar correspondence for angles is not very clear. In the deep semiclassical limit one expects a correspondence but the problem at hand is far from such a limit. Second observation is that the quantum dynamics associated with a particular ZOBS, semiclassically speaking, would naturally involve a family of classical trajectories which are modeled here with the random angle distributions. The

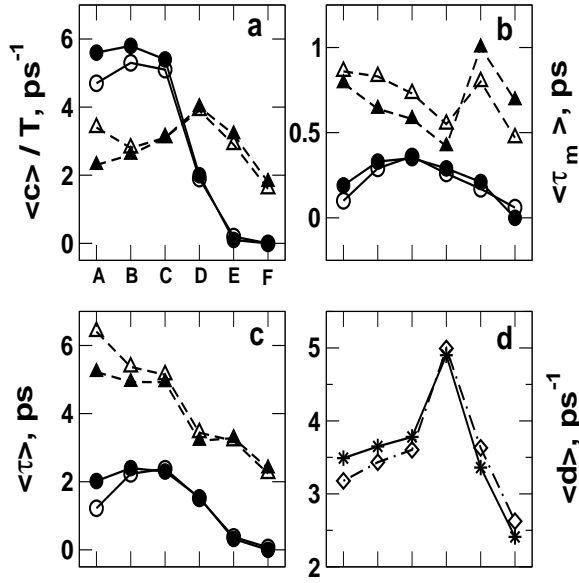


FIG. 8: Average crossings per unit time (a), average longest locking time (b), total time near a specific resonance (c) and diffusion of the frequencies (d) are shown in this figure for six ZOBS. A, B, C, D, E, F correspond to the bright states $|030\rangle, |040\rangle, |050\rangle, |006\rangle, |008\rangle$, and $|0010\rangle$ respectively. Averaging is done over 1000 trajectories and $T = 10$ ps. In (a), (b), and (c) the filled circles and triangles correspond to the mn and mbb resonances respectively while the open symbols are for the case with $k_{nbb} = 0$. See text for details.

fact that the diffusion of the frequency ratios are strongly dependent on the choice of the phase space slice further support the procedure of angle averaging. The quantities of interest are number of crossings per unit time of the two main resonances (denoted $\langle c_{mn}, c_{mbb} \rangle / T$), total time spent near the resonances (denoted $\langle \tau_{mn}, \tau_{mbb} \rangle$), longest locking time in a given resonance (denoted $\langle \tau_m \rangle$), and the diffusions $d(T)$. In this study we have averaged over 1000 trajectories with the angles chosen such that $E = E_{ZOBS} \pm 1.0 \text{ cm}^{-1}$ and each trajectory was propagated to $T = 10$ ps.

In Fig.8 we show the various dynamical quantities of interest for three of the experimental CO stretch bright states and three of the bend only bright states corresponding to the polyads $P = 3, 4, 5$. In Fig.8a the number of resonance crossings per unit time are shown. It is immediately clear that the mn resonance plays a dominant role for the CO stretch bright states and that the mbb resonance is key for the bend bright states. Notice that for the $|008\rangle$ and the $|0010\rangle$ bright states the ‘flux’ across mn is almost zero. On the other hand despite the dominance of mn flux for the CO stretch ZOBS, the mbb flux is not negligible. This already provides a hint to the drastically different IVR dynamics from the two classes of ZOBS with $|003\rangle$ being an exception. Fig.8b shows the longest locking time, on average, for the different bright states. Interestingly even though the mn flux is larger than the mbb flux for the CO stretch states

the τ_m ’s show the opposite trend. The total time spent near a particular resonance as shown in Fig.8c also indicates that the IVR from CO stretch states is strongly effected by the mbb resonance. The diffusions in Fig.8d show marginal differences. A clear picture emerges for the IVR dynamics associated with the CO stretch bright states. Initially the mn resonance transfers energy to the DC stretch (dissociation mode) but prior to a substantial buildup of excitation in the DC stretch the energy is “siphoned off” into the bend mode via the mbb resonance. This process happens for a fairly long time leading to a highly nonstatistical nature of the dynamics and unimolecular decay of DCO. On the other hand for the bend bright states corresponding to $P = 4, 5$ the initial IVR dynamics is dominated by the mbb resonance. However the mn resonance is unable to compete and this results in unhindered transfer of energy to the dissociative mode via the mbb coupling. Exception to the nature of bend ZOBS is clearly seen in the case of $|006\rangle$ wherein the mn resonance does compete and leads to transfer of energy from the dissociative mode to the CO stretch mode. An important observation is that the diffusion of frequencies computed here is the lowest for the ZOBS $|0010\rangle$ which undergoes the fastest unimolecular decay. This is not a contradiction since large diffusion corresponds to many hops and consequent locking leading to incomplete flow of energy into the dissociative mode. For example the largest diffusion is predicted for the ZOBS $|006\rangle$ which is consistent with the fact that the times spent near the two main resonances are similar as compared to the other states. Thus $|006\rangle$ should decay the slowest which is confirmed by computing the associated survival probability (cf. figure 3(b) in Ref. 20). It is interesting to observe that the diffusions for the CO stretch bright states are not very different whereas in the case of the bend bright states there is a large variation. This demonstrates the mode-specificity of the intramolecular dynamics of DCO.

In Fig.8 the effect of setting $k_{nbb} = 0$ is shown. It is clear that the largest effect of the nbb Fermi resonance is for the CO stretch bright states $|030\rangle$ and $|040\rangle$. In the absence of nbb the mn flux is decreased and the mbb flux is increased with larger time being spent, on the average, near the mbb Fermi resonance. This indicates that the CO stretch bright states would lead to smaller rates of unimolecular decay in the absence of the nbb resonance. This is true for the bend bright states as well although the effect is very small. Thus the role of nbb Fermi resonance is not negligible for the lower polyads. As a final observation we point out that amongst the CO stretch bright states there is a sharp increase, on going from $|030\rangle$ to the $|040\rangle$, in the average residence time and the average longest locking time for the mn resonance. This perhaps explains the efficiency of the mn resonance in $P = 4$ but at this stage it is conjectural.

V. CONCLUSIONS

A long term goal of our research is to come up with techniques that would allow fairly detailed classical-quantum correspondence studies of highly excited states in systems with three degrees of freedom or more. To this end two dimensionality independent techniques, parametric variations and local frequency analysis, have been employed in this study. We have demonstrated the utility of both the techniques for understanding the intramolecular dynamics of DCO. The successes of both the techniques, in dynamical assignments of states and establishing the nonstatistical nature of the dynamics, given the strongly coupled nature of the system (coupling strengths comparable to the mean level spacing) is quite encouraging. We conclude with brief comments on the techniques and future outlook.

The level velocity approach, used to dynamically assign the eigenstates, is certainly capable of identifying strongly localized states. The close connections between the level velocity of an eigenstate and its corresponding phase space nature makes this approach attractive. Previous application⁵⁰ to a mixed 2-mode system demonstrated the utility of the level velocities for dynamical assignments of the highly excited states. In this work we have shown that the method is useful even in the presence of significant chaos. Although avoided crossings lead to difficulties, and this is not surprising, it is debatable whether the resulting mixed states can be or should be assigned. Demixing the states involved in avoided crossings and then analyzing them can be done within this approach as in any other approach. However the procedure of demixing, especially in multistate or broad avoided crossings, should not be considered as an assignment. This work shows that analyzing the level velocities in conjunction with measures like IPRs can be a fairly useful way of dynamically assigning highly excited states. At this stage the effects of various bifurcations on the level velocity spectrum is not known. Interestingly in the case of DCO, despite substantial change in the phase space structure with changing energies, the level velocity corresponding to a state localized about stable regions is very close to the classical estimate. This has been observed before⁵⁰ in the case of HCP as well. This suggests a very detailed classical-quantum correspondence and needs to be studied further. In order to make this approach more useful it is important to obtain some bounds on the level velocities in the mixed and strongly chaotic situations. Thus a semiclassical theory for the velocities in the chaotic regimes needs to be developed and work is in progress in our group along these lines. Note that the distribution of the velocities has been found to be gaussian in the strong chaos limit⁷⁰. The general technique of parametric variations has a wide range of applications and level curvatures have also been studied⁷⁰. It remains to be seen if the level curvatures have any utility in understanding highly excited states and IVR. For example conductance of disordered systems have been related to

level curvatures^{54,70,71} and given the tantalizing similarities between the example mentioned and IVR it seems worthwhile to investigate the utility of level curvatures in molecular systems.

The LFA technique is able to provide detailed phase space information in a strongly coupled system like DCO. In particular the time-frequency analysis revealed the existence of trajectories trapped near important resonance zones. In an effective spectroscopic Hamiltonian the key resonances are easy to expect since the fit already builds in the main resonant perturbations but LFA is able to provide information on the competing roles of these various resonances. An example is the clear differences between the CO-stretch bright state and DCO bend bright state dynamics for DCO. LFA is also able to highlight the role of weak resonances like the *nbb* Fermi resonance. As shown in this work and in the previous works the wavelet based approach to LFA is useful in analyzing effective Hamiltonians and various dynamical quantities can be determined to understand IVR. LFA clearly shows that despite significant chaos the DCO phase space is far from the RMT regime. In this paper it is shown that even for a strongly coupled system like DCO the state space diffusion has a lot of structure with regions of high and low diffusions interspersed throughout. The diffusion of frequencies provides clear insights into the dynamics at a particular polyad and/or a specific energy. This information can then be used to determine the nature of the 'random walk' in action space for strongly coupled systems and thus provide more insights into certain recent conjectures⁶⁷ regarding the intermediate time behavior of survival probabilities. Although not shown here most of the trajectories exhibit across-resonance diffusion which is quite fast and implicates higher order secondary resonances as well^{45,72}. The rapid frequency jumps which perhaps correspond to heteroclinic orbits joining unstable periodic orbits have not been investigated in detail. Surely the rapid jumps from one resonance to another have important consequences for IVR and needs further study. We also note that there is not much of an Arnol'd web for DCO for $P = 3, 4$ in contrast⁴⁷ to H₂O. DCO being effectively two dimensional implies that there is no transport along resonance lines and thus many of the interesting conjectures put forward^{41,42} by Martens, Davis, and Ezra remain to be tested. Currently work is in progress for true three degree of freedom systems.

As a final note we mention that both techniques used in the current study probe localization characteristics. The parametric response is probing eigenstate localization and the LFA is probing localization of phase space transport due to partial barriers and broken separatrices. Localization explicitly implies nonstatistical behavior and thus deviations from RMT and incomplete IVR in the system. Evidence exists^{73,74} that the quantized versions of the partial barriers can be more restrictive than the classical analogs. A interesting link between these two approaches is provided by the recently proposed intensity-velocity correlator^{51,52,53}. Detailed studies of

true three degrees of freedom system via the intensity-velocity correlator can lead to a better understanding of the IVR dynamics.

VI. ACKNOWLEDGEMENTS

It is a pleasure to acknowledge useful discussions with Dr. L. V. Arevalo regarding the wavelet based approach

to time-frequency analysis. We are also grateful to Prof. Greg Ezra for sending us a copy of the unpublished work Ref.42. This work is supported by funds from the Department of Science and Technology, India.

-
- ¹ M. Bixon and J. Jortner, *J. Chem. Phys.* **48**, 715 (1968).
² S. A. Rice, *Adv. Chem. Phys.* **47**, 117 (1981).
³ T. Uzer, *Phys. Rep.* **199**, 73 (1991).
⁴ K. K. Lehmann, G. Scoles, and B. H. Pate, *Annu. Rev. Phys. Chem.* **45**, 241 (1994).
⁵ D. J. Nesbitt and R. W. Field, *J. Phys. Chem.* **100**, 12735 (1996).
⁶ M. Gruebele and R. Bigwood, *Int. Rev. Phys. Chem.* **17**, 91 (1998).
⁷ M. Gruebele, *Adv. Chem. Phys.* **114**, 193 (2000).
⁸ J. C. Keske and B. H. Pate, *Annu. Rev. Phys. Chem.* **51**, 323 (2000).
⁹ M. Gruebele, *Theor. Chem. Acc.* **109**, 53 (2003).
¹⁰ T. Baer and W. L. Hase, *Unimolecular Reaction Dynamics: Theory and Experiments*, Oxford University press, Oxford, 1996.
¹¹ J. S. Hutchinson, E. L. Sibert III, and J. T. Hynes, *J. Chem. Phys.* **81**, 1314 (1984).
¹² A. A. Stuchebrukhov and R. A. Marcus, *J. Chem. Phys.* **98**, 8443 (1993).
¹³ R. T. Lawton and M. S. Child, *Mol. Phys.* **37**, 1799 (1979).
¹⁴ M. J. Davis and E. J. Heller, *J. Chem. Phys.* **75**, 246 (1981).
¹⁵ E. J. Heller, *J. Phys. Chem.* **99**, 2625 (1995).
¹⁶ S. Keshavamurthy, *J. Chem. Phys.* **119**, 161 (2003).
¹⁷ See C. Stöck, X. Li, H. -M. Keller, R. Schinke, and F. Temps, *J. Chem. Phys.* **106**, 5333 (1997) and references therein.
¹⁸ H. -M. Keller, M. Stumpf, T. Schröder, C. Stöck, F. Temps, R. Schinke, H. -J. Werner, C. Bauer, and P. Rosmus, *J. Chem. Phys.* **106**, 5359 (1997).
¹⁹ S. Stamatiadis, S. C. Farantos, H. -M. Keller, and R. Schinke, *Chem. Phys. Lett.* **344**, 565 (2001).
²⁰ F. Renth, F. Temps, and A. Trölsch, *J. Chem. Phys.* **118**, 659 (2003).
²¹ C. Jung, H. S. Taylor, and E. Atilgan, *J. Phys. Chem. A* **106**, 3092 (2002).
²² A. Trölsch and F. Temps, *Z. Phys. Chem. (Munich)* **215**, 207 (2001).
²³ See R. E. Wyatt and C. Iung in *Dynamics of Molecules and Chemical Reactions* Eds. R. E. Wyatt and J. Z. H. Zhang, pp 59, Marcel Dekker, NY, 1996.
²⁴ A. A. Stuchebrukhov, A. Mehta, and R. A. Marcus, *J. Phys. Chem.* **97**, 12491 (1993).
²⁵ D. V. Shalashilin and M. S. Child, *J. Chem. Phys.* **119**, 1961 (2003).
²⁶ M. E. Kellman, *Annu. Rev. Phys. Chem.* **46**, 395 (1995); G. S. Ezra, *Adv. Class. Traj. Meth.* **1**, 1 (1992); M. J. Davis, *Int. Rev. Phys. Chem.* **14**, 15 (1995); G. S. Ezra, *Adv. Class. Traj. Meth.* **3**, 35 (1998) and references therein;
B. I. Zhilinskii, *Phys. Rep.* **341**, 85 (2001); M. S. Child, *J. Molec. Spec.* **210**, 157 (2001); M. J. Davis, *Int. Rev. Phys. Chem.* **14**, 15 (1995); M. P. Jacobson and R. W. Field, *J. Phys. Chem. A* **104**, 3073 (2000); M. Joyeux, S. C. Farantos, and R. Schinke, *J. Phys. Chem. A* **106**, 5407 (2002).
²⁷ E. L. Sibert III, W. P. Reinhardt, and J. T. Hynes, *J. Chem. Phys.* **81**, 1115 (1984).
²⁸ Z. Lu and M. E. Kellman, *J. Chem. Phys.* **107**, 1 (1997).
²⁹ S. Keshavamurthy and G. S. Ezra, *J. Chem. Phys.* **107**, 156 (1997).
³⁰ S. Keshavamurthy and G. S. Ezra, *Chem. Phys. Lett.* **259**, 81 (1996).
³¹ M. P. Jacobson, C. Jung, H. S. Taylor, and R. W. Field, *J. Chem. Phys.* **111**, 600 (1999).
³² H. Ishikawa, R. W. Field, S. C. Farantos, M. Joyeux, J. Koput, C. Beck, and R. Schinke, *Annu. Rev. Phys. Chem.* **50**, 443 (1999).
³³ C. Jung, E. Ziemniak, and H. S. Taylor, *J. Chem. Phys.* **115**, 2499 (2001).
³⁴ C. C. Martens and W. P. Reinhardt, *J. Chem. Phys.* **93**, 5621 (1990).
³⁵ C. C. Martens, *J. Stat. Phys.* **68**, 207 (1992).
³⁶ K. M. Atkins and D. E. Logan, *J. Chem. Phys.* **97**, 2438 (1992).
³⁷ See P. Lochak in *Hamiltonian Systems with Three or More Degrees of Freedom*, Ed. C. Simó, pp 168, NATO ASI Series, Kluwer, Dordrecht, 1999 and references therein.
³⁸ G. Contopoulos, S. C. Farantos, H. Papadaki, C. Polymilis, *Phys. Rev. E* **50**, 4399 (1994).
³⁹ R. E. Gillilan and G. S. Ezra, *J. Chem. Phys.* **94**, 2648 (1991).
⁴⁰ D. Begie, *J. Nonlinear Sci.* **5**, 57 (1995).
⁴¹ C. C. Martens, M. J. Davis, and G. S. Ezra, *Chem. Phys. Lett.* **142**, 519 (1987).
⁴² C. C. Martens, M. J. Davis, and G. S. Ezra, unpublished.
⁴³ D. Carter and P. Brumer, *J. Chem. Phys.* **77**, 4208 (1982).
⁴⁴ M. J. Davis, *J. Chem. Phys.* **83**, 1016 (1985).
⁴⁵ J. Laskar, *Physica D* **67**, 257 (1993); See J. Laskar in *Hamiltonian Systems with Three or More degrees of Freedom*, pp 134, NATO-ASI, Kluwer Dordrecht, 1999.
⁴⁶ J. von Milczewski, D. Farrelly, and T. Uzer, *Phys. Rev. Lett.* **78**, 1436 (1997).
⁴⁷ L. V. Vela-Arevalo and S. Wiggins, *Int. J. Bifurcations and Chaos* **11**, 1359 (2001).
⁴⁸ J. C. Losada, J. M. Estebaranz, and R. M. Benito, *J. Chem. Phys.* **108**, 63 (1998).
⁴⁹ L. V. Vela-Arevalo, *Time-Frequency analysis based on wavelets for Hamiltonian systems*, Ph.D. Thesis, Caltech, 2002.

- ⁵⁰ A. Semparithi, V. Charulatha, and S. Keshavamurthy, *J. Chem. Phys.* **118**, 1146 (2003).
- ⁵¹ S. Tomsovic, *Phys. Rev. Lett.* **77**, 4158 (1996); N. R. Cerruti, A. Lakshminarayan, J. H. Lefebvre, and S. Tomsovic, *Phys. Rev. E* **63**, 016208 (2001); A. Lakshminarayan, N. R. Cerruti, and S. Tomsovic, *Phys. Rev. E* **63**, 016209 (2001).
- ⁵² S. Keshavamurthy, N. R. Cerruti, and S. Tomsovic, *J. Chem. Phys.* **117**, 4168 (2002).
- ⁵³ N. R. Cerruti, S. Keshavamurthy, and S. Tomsovic, *Phys. Rev. E* (2003), submitted.
- ⁵⁴ D. J. Thouless, *Phys. Rep.* **13C**, 93 (1974).
- ⁵⁵ See for example, K. Tsiganis, A. Anastasiadis, and H. Varvoglis, *Chaos, Solitons and Fractals* **11**, 2281 (2000) and references therein; A. Iomin and G. M. Zaslavsky, *Chem. Phys.* **284**, 3 (2002); B. J. West, *Chem. Phys.* **284**, 45 (2002).
- ⁵⁶ B. V. Chirikov, *Phys. Rep.* **52**, 263 (1979).
- ⁵⁷ S. Keshavamurthy, *J. Phys. Chem. A* **105**, 2668 (2001).
- ⁵⁸ M. V. Berry, *Philos. Trans. R. Soc. London* **287**, 237 (1977); M. V. Berry, *J. Phys. A* **10**, 2083 (1977).
- ⁵⁹ A. Voros in *Stochastic behaviour in Classical and Quantum Hamiltonian Systems* (Lecture Notes in Physics 93), pp 326 Ed. G. Casati and J. Ford, Springer, NY 1979.
- ⁶⁰ A. M. Ozorio de Almeida, *Hamiltonian Systems: Chaos and Quantization* (Cambridge University Press, Cambridge, 1988).
- ⁶¹ L. Kaplan and E. J. Heller, *Ann. Phys. (Leipzig)* **264**, 171 (1998).
- ⁶² B. Eckhardt, S. Fishman, K. Müller, and D. Wintgen, *Phys. Rev. A* **45**, 3531 (1992).
- ⁶³ M. V. Berry and M. Tabor, *Proc. R. Soc. London Ser. A* **349**, 101 (1976).
- ⁶⁴ A. M. Ozorio de Almeida in *Quantum Chaos and Statistical Nuclear Physics*, Ed. T. H. Seligman and H. Nishioka, Lecture Notes in Physics 263 (Springer, Berlin, 1986); D. Ullmo, M. Grinberg, and S. Tomsovic, *Phys. Rev. E* **54**, 136 (1996).
- ⁶⁵ M. C. Gutzwiller, *J. Math. Phys.* **12**, 343 (1971).
- ⁶⁶ This is a generalization of the familiar semiclassical matrix elements in one dimension wherein the quantum mean value of an observable is expressed as a classical time average of the observable over the period of a mean orbit. See M. S. Child, *Semiclassical Mechanics with Molecular Applications*, section 5.2, Clarendon Press, Oxford, 1991.
- ⁶⁷ S. A. Schofield, R. E. Wyatt, and P. G. Wolynes, *J. Chem. Phys.* **105**, 940 (1996); V. Wong and M. Gruebele, *J. Phys. Chem. A* **103**, 10083 (1999); S. Keshavamurthy, *Chem. Phys. Lett.* **300**, 281 (1999).
- ⁶⁸ J. D. Meiss, *Rev. Mod. Phys.* **64**, 795 (1992) and references therein; R. S. Mackay and J. D. Meiss, *Hamiltonian Dynamical Systems*, see part 6, Adam Hilger, Bristol, 1987.
- ⁶⁹ Y. Meyer, *Wavelets: Algorithms and Applications*, SIAM, Philadelphia, 1993.
- ⁷⁰ See F. Haake, *Quantum Signatures of Chaos*, chapter 6, 2nd ed. (Springer, Berlin, 2000).
- ⁷¹ D. Braun, E. Hofstetter, A. MacKinnon, and G. Montambaux, *Phys. Rev. B* **55**, 7557 (1997); D. Braun and G. Montambaux, *Phys. Rev. B* **50**, 7776 (1994); Y. V. Fyodorov and H. -J. Sommers, *Phys. Rev. E* **51**, R2719 (1995).
- ⁷² G. Haller, *Phys. Lett. A* **200**, 34 (1995).
- ⁷³ G. Radons, T. Geisel, and J. Rubner, *Adv. Chem. Phys.* **LXXIII**, 891 (1989).
- ⁷⁴ R. C. Brown and R. E. Wyatt, *Phys. Rev. Lett.* **57**, 1 (1986).